Origin of the Single Chain Magnet Behavior of the Co(H 2 L)(H 2 O) Compound with a 1D Structure

ARTICLE *in* THE JOURNAL OF PHYSICAL CHEMISTRY A · JANUARY 2007

Impact Factor: 2.69 · DOI: 10.1021/jp063871p · Source: PubMed

9 AUTHORS, INCLUDING:

Andrei V Palii
Academy of Sciences of Moldova
77 PUBLICATIONS **1,155** CITATIONS
SEE PROFILE

Hanhua Zhao
Texas A&M University
113 PUBLICATIONS **2,556** CITATIONS
SEE PROFILE

Jiang-Gao Mao
Chinese Academy of Sciences
283 PUBLICATIONS **5,877** CITATIONS
SEE PROFILE

Kim R Dunbar
Texas A&M University
442 PUBLICATIONS **13,322** CITATIONS
SEE PROFILE

Origin of the Single Chain Magnet Behavior of the $Co(H_2L)(H_2O)$ Compound with a 1D Structure

Andrei V. Palii,[†] Sergei M. Ostrovsky,[†] Sophia I. Klokishner,*[,†] Oleg S. Reu,[†] Zhong-Ming Sun,[‡] Andrei V. Prosvirin,[§] Han-Hua Zhao,[§] Jiang-Gao Mao,[§] and K. R. Dunbar*[,§]

Institute of Applied Physics of the Academy of Sciences of Moldova, Academy str.5, Kishinev MD 2028, Moldova, State Key Laboratory of Structural Chemistry, Fujian Institute of Research on the Structure of Matter, Chinese Academy of Sciences, Fuzhou 350002, P. R. China, and Department of Chemistry, Texas A&M University, P.O. Box 30012, College Station, Texas 77843-3012

Received: June 21, 2006; In Final Form: October 24, 2006

The paper is aimed at the elucidation of the main factors responsible for the single-chain magnet behavior of the cobalt(II) disphosphonate compound $Co(H_2L)(H_2O)$ with a 1D structure. The model takes into account the spin−orbit interaction, the axial component of the octahedral crystal field acting on the ground-state cubic $^4T_1$ terms of the Co(II) ions, the antiferromagnetic exchange interaction between Co(II) ions as well as the difference in the crystallographic positions of these ions. The conditions that favor the single-chain magnet behavior based on spin canting in a 1D chain containing inequivalent Co(II) centers are discussed. The peculiarities of this behavior in chains containing orbitally degenerate ions are revealed. The qualitative explanation of the experimental data is given.

1. Introduction. Short Overview of Experimental Results

The most fascinating developments of the past decade in the field of molecule-based magnetism involve the discovery and characterization of single molecule magnets (SMMs)[1−11] and single-chain magnets (SCMs).[12−19] Magnetic bistability and slow magnetic relaxation at low temperatures are the distinctive features of these systems that may lead to future trends for wide applications in quantum and molecular electronics. The majority of known SMMs and SCMs contain ions with orbitally nondegenerate ground states. For SMMs of this type the energy barrier for magnetization reversal appears as a result of the combination of the large spin S of the ground state and a significant negative zero-field spliiting D_S, whereas the relaxation time of magnetization exhibits a thermally activated behavior (Arrhenius law)

$$\tau_i(T) = \tau_0 \exp\left(\frac{|D_S|S^2}{kT}\right) \quad (1)$$

In accordance with the Glauber model[20] for SCMs in which individual anisotropic units possessing ground states with quenched orbital angular momenta are coupled by ferromagnetic exchange, the relaxation time also depends on the exchange integral J_F of this interaction

$$\tau(T) = \tau_i(T) \exp\left(\frac{8J_FS^2}{kT}\right) \quad (2)$$

In an attempt to increase both the energy barrier for magnetization reversal and the lifetime of magnetization, researchers have turned to new types of SMMs[11,21,22] and SCMs that contain ions with unquenched orbital angular momenta in the ground state. Recently we demonstrated[23−25] that for the SMM of this kind, the first−order single ion anisotropy and the anisotropy of exchange interaction are responsible for the formation of the barrier for reversal of magnetization. As for the SCM containing orbitally degenerate ions, the state of experiment and theory is very scarce. Only a few examples of such type systems have been reported.[26,27]

In the cobalt(II) diphosphonate $Co(H_2L)(H_2O)$ compound which displays SCM properties[26] the Co(II) ions are linked through a bridging phosphonate oxygen atom to create a 1D chain of corner-sharing octahedra that propagate in a zigzag fashion (Figure 1). The crystallographic positions of neighboring Co(II) ions in the chain are inequivalent, however, due to the fact that the corresponding ligand octahedra are rotated with respect to each other. It will be demonstrated in this paper that this situation results in a noncollinear spin structure (spin canting). At the same time the two cobalt centers in the chain present identical environments and are linked to five oxygen and one nitrogen atoms. The χT vs T plot of the cobalt(II) diphosphonate compound $Co(H_2L)(H_2O)$ (Figure 2) exhibits a room-temperature value of 3.2 emu·mol^{-1}·K, which is higher than the expected value for a spin-only case (χT = 1.8 emu·mol^{-1}·K, $S = {}^3/_2$). Upon lowering the temperature, the χT value decreases and reaches a minimum of 0.6 emu·mol^{-1}·K at 7 K. Below 7 K, χT increases abruptly to reach a maximum at ∼2.5 K (χT = 2.5 emu·mol^{-1}·K) and finally decreases again at lower temperatures. The observed χT behavior indicates an antiferromagnetic exchange interaction between the Co ions and the origin of the χT maximum at ∼2.5 K is attributed to spin canting. The SCM behavior of the title compound is evidenced by the temperature dependence of the *ac* susceptibility for which both the real and imaginary components are strongly frequency dependent (Figure 3).[26]

* Corresponding authors. E-mail: S.I.K., klokishner@yahoo.com; K.R.D., dunbar@mail.chem.tamu.edu.
[†] Academy of Sciences of Moldova.
[‡] Chinese Academy of Sciences.
[§] Texas A&M University.

10.1021/jp063871p CCC: $33.50
Published on Web 12/21/2006

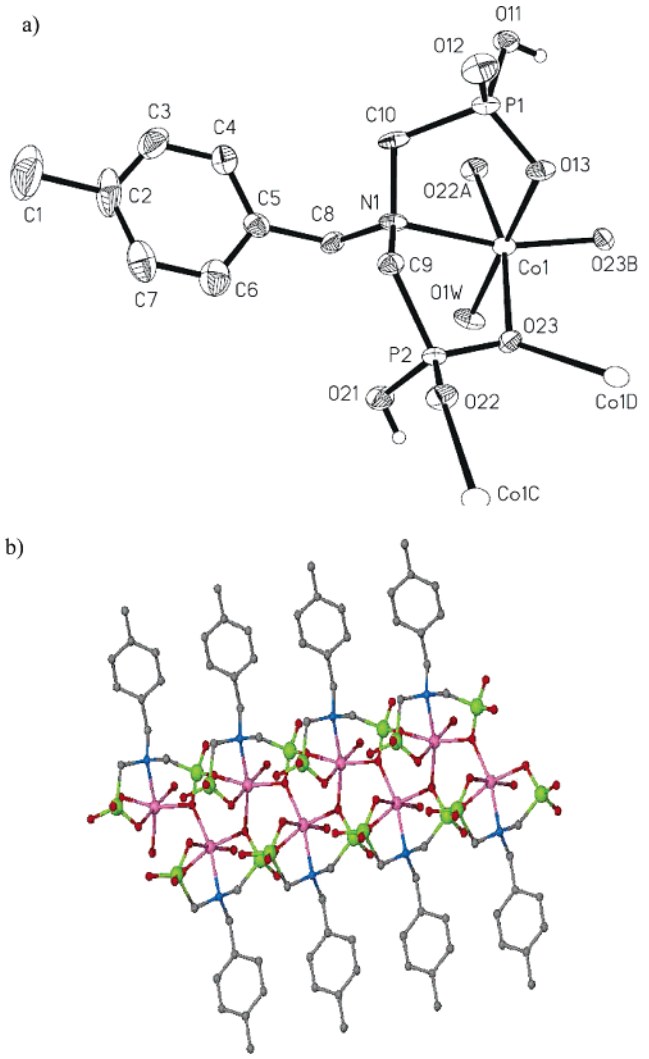

Figure 1. (a) ORTEP representation of the $Co(H_2L)(H_2O)$ unit. The thermal ellipsoids are drawn at the 50% probability level. (b) Extension of the view in (a) down the *c*-axis to emphasize the zigzag chain structure. The Co and P atoms are shaded in pink and green, respectively.

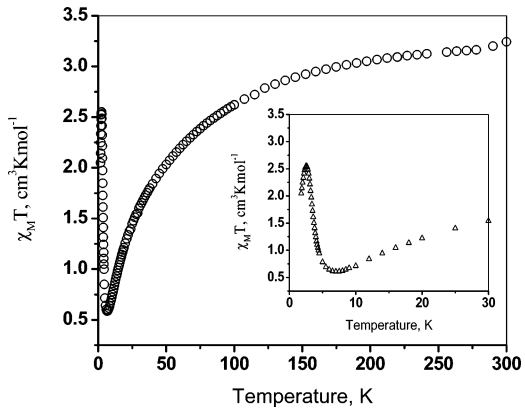

Figure 2. Temperature dependence of χT for the $Co(H_2L)(H_2O)$ compound. The inset shows the low-temperature part of χT.

In striving to understand the SCM behavior of the $Co(H_2L)(H_2O)$ chain compound we note that, in a first approximation, the nearest octahedral surrounding of the Co(II) ion is tetragonally distorted.[26] The tetragonal component of the crystal field splits the ground $^4T_1$ term of the Co(II) ion into the orbital singlet $^4A_2$ and the orbital doublet ^4E. The description of the ground

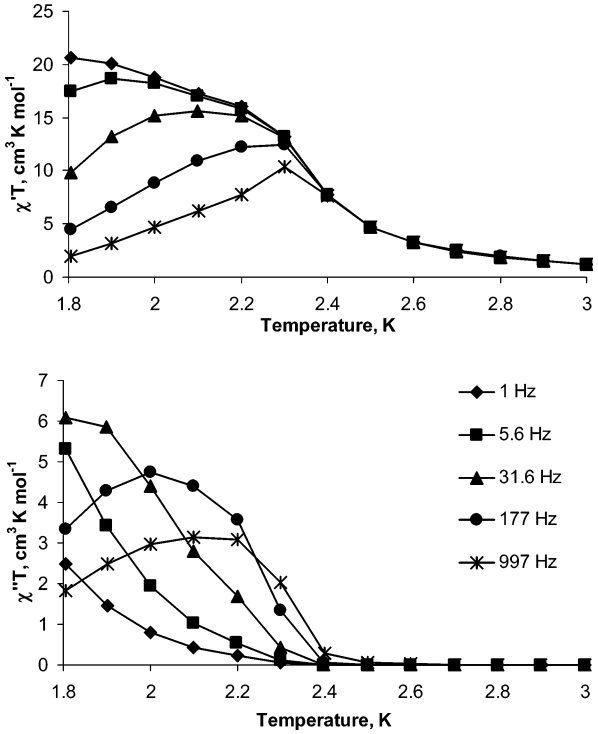

Figure 3. Temperature dependence of the χ' (top) and χ'' (bottom) components of the ac susceptibility with an oscillating field of 3 Oe at fixed frequencies. The lines are guides for the eye.

state splitting by the zero field splitting Hamiltonian $D_S[S_Z^2 - (1/3)S(S+1)]$ proves to be only valid when the ground state is $^4A_2$ and it is well separated from the ^4E state (strong tetragonal field). However, the observed room-temperature χT value indicates the presence of an unquenched orbital momentum of the Co(II) ions in the $Co(H_2L)(H_2O)$ compound. Thus, in examining the magnetic properties of this compound, one must deal with a significant local (single-ion) anisotropy that cannot be described by the term $D_S[S_Z^2 - (1/3)S(S+1)]$. Besides this problem, the role of spin canting in the formation of an uncompensated magnetic moment in a chain with antiferromagnetic coupling must also be elucidated. The relaxation time of magnetization for the title compound does not obey the law, eq 2. The above arguments clearly show that the conventional model based on the spin-Hamiltonian, which involves the isotropic exchange interaction between the Co(II) ions in the chain and a zero-field splitting term fails for the description of the magnetic properties of the Co(II) chain compound in this study. The aim of this paper is to provide insight into the interplay between the local anisotropy of the Co(II) ions possessing the unquenched orbital momenta, antiferromagnetic exchange interaction between these ions, and spin canting. The influence of these key factors on the magnetic properties and SCM behavior of the Co(II) chain will be considered. We will elaborate a new approach that can be used to analyze the SCM properties of 1D chains containing orbitally degenerate Co(II) ions. Within the framework of the proposed approach special emphasis will be placed on the qualitative interpretation of the experimental data on the $Co(H_2L)(H_2O)$ chain compound.

2. Pseudo-Spin-$^1/_2$ Hamiltonian for a Pair of Octahedrally Coordinated Co(II) ions Exhibiting Spin Canting

The method of the effective pseudo-spin-$^1/_2$ Hamiltonian is widely used for the description of the magnetic and spectroscopic properties of compounds comprising exchange coupled

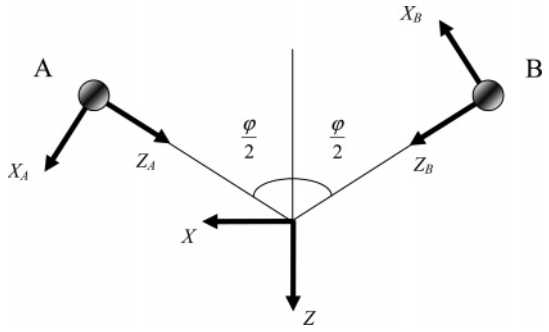

Figure 4. Local and molecular coordinates.

Co(II) ions. As a rule, such type Hamiltonians are constructed on the basis of symmetry arguments, and the parameters of the Hamiltonian are determined from fitting of the experimental data (phenomenological approach).[28−32] In the approach recently developed[33,34] the parameters of the effective Hamiltonian are expressed through the set of microscopic parameters (spin−orbit coupling constant, low-symmetry crystal field parameters and Heisenberg exchange integral). However, until now this approach has been applied to Co(II) ions that occupy identical crystallographic positions. Herein we go beyond this simplifying assumption and consider a pair of Co(II) ions, the octahedral surroundings of which is tetragonally distorted and rotated with respect to each other. A similar procedure for calculations of the energy pattern for a trimeric Co(II) complex by means of the second-order perturbation theory was performed in[35] without usage of the pseudo-spin-$^1/_2$ Hamiltonian.

Let us assign the indices A and B to two octahedrally coordinated Co(II) ions which occupy inequivalent crystallographic positions in a 1D chain. We introduce two local frames of reference (Figure 4) relating to ions A and B in the chain. To demonstrate the effects of spin canting in the chain with utmost clarity, we assume that the tetragonal local Z_A and Z_B axes subtend an angle φ each of them passing through a Co and nitrogen atom, the Y_A and Y_B axes are parallel to each other and perpendicular to Z_AZ_B plane, and the axes X_A and X_B lie in the Z_AZ_B plane. The B center system axes can be obtained from the A center system axes by the φ degree turn around the Y_A or Y_B axis. Along with the local frames of reference we introduce the molecular coordinates. The Z axis of this system is chosen along the bisector of the angle φ formed by the local Z_A and Z_B axes and the Y axis of the molecular system coincides with the local Y_A and Y_B axes (Figure 4).

The single −ion Hamiltonian can be presented as follows:

$$\mathbf{H}_i = -(3/2)\kappa\lambda\mathbf{l}_i\mathbf{s}_i + \Delta[l_{iZ}^2(i) - {}^2/_3] + \hat{H}_{ZE}^i \qquad i = A, B \quad (3)$$

where the first term represents the spin−orbit interaction (λ is the many-electron spin−orbit coupling parameter for the $^4T_1$-term of the Co(II) ion, κ is the orbital reduction factor), the second term describes the local axial crystal field acting on each Co(II) ion, and the last term

$$H_{ZE}^i = \beta \sum_{\gamma=X,Y,Z} [-{}^3/_2\kappa l_{i\gamma}(i) + g_e s_{i\gamma}(i)]H_\gamma(i) \qquad (4)$$

is the operator of Zeeman interaction, wherein β is the Bohr magneton, and **H** is the applied magnetic field. In developing the Hamiltonian eq 3, we consider that for ions A and B the local axes coincide with the main axes of the tensor that describes the splitting of the $^4T_1$ term in the local crystal field, and the local surroundings of these ions are identical. Index i in the parentheses in eqs 3 and 4 indicates that the angular momenta operators and magnetic field components are defined in the local frame associated with the site i (i = A, B).

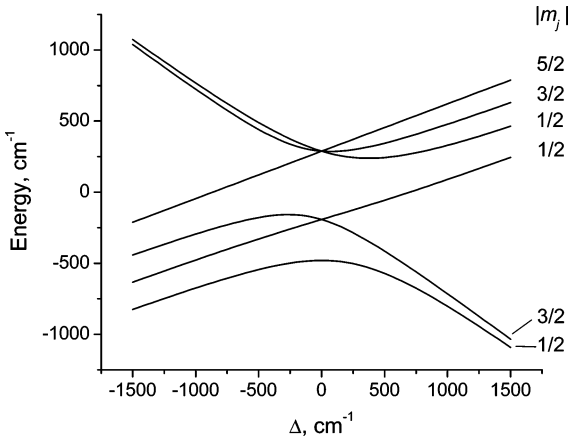

Figure 5. Energy levels of the Co ion in the axial surrounding for $\lambda = -160$ cm^{-1}, $\kappa = 0.8$.

The single-ion wavefunctions in the total angular momentum representation are obtained by the Clebsch-Gordan decomposition $|j, m_j\rangle = \sum_{m_l m_s} \mathbf{C}^{jm_j}_{1m_l,{}^3/_2 m_s}|1m_l,{}^3/_2 m_s\rangle$, where m_s and m_l are the projections of the total spin $S = {}^3/_2$ of the Co(II) ion and its angular momentum $l = 1$, respectively, j and m_j represent the total angular momentum of the Co(II) ion and its projection. Because j takes on the values $j = {}^1/_2, {}^3/_2, {}^5/_2$, the Hamiltonian H_i is represented by the 12 × 12 matrix. The diagonalization of this matrix gives 6 Kramers doublets.

In Figure 5 the energies of these states in the absence of the external magnetic field are shown as functions of the axial crystal field parameter Δ for usually accepted values of $\lambda = -160$ cm^{-1}, $\kappa = 0.8$. From Figure 5 it is seen that for a wide range of Δ values the ground Kramers doublet is well separated from the excited states. This allows us to describe the energy pattern of the low-lying levels of the exchange coupled Co(II) pair by a pseudo-spin-$^1/_2$ Hamiltonian acting within the space of the direct product of two Kramers doublets. The wavefunctions $\Psi_{gr}(\pm{}^1/_2)$ for the ground Kramers doublet represent linear combinations of the states $|j = {}^1/_2, m_j = \pm{}^1/_2\rangle$, $|j = {}^3/_2, m_j = \pm{}^1/_2\rangle$ and $|j = {}^5/_2, m_j = \pm{}^1/_2\rangle$, with the coefficients being dependent on the parameters λ, κ and Δ.

Along with the intracenter interactions described by eq 3 the full Hamiltonian of the Co(II) pair includes the exchange interaction between Co(II) ions. Following the idea of Lines,[36] we will assume the isotropic Heisenberg−Dirac−Van Vleck (HDVV) form of this interaction

$$H_{ex} = -2Js_As_B = -2\,J(s_X^As_X^B + s_Y^As_Y^B + s_Z^As_Z^B) \qquad (5)$$

where J is the many-electron exchange parameter and the single ion spin operators s_A and s_B and their projections s_α^A and s_α^B ($\alpha = X, Y, Z$) refer to the common (molecular) frame.

Now we pass from the operators s_α^A, s_α^B ($\alpha = X, Y, Z$) to the operators $s_X^i(i)$, $s_Y^i(i)$, $s_Z^i(i)$, i = A, B, defined in the local coordinates (see eq A1 in Appendix). Then the exchange Hamiltonian takes on the form

$$H_{ex} = -2J\{s_Y^A(A)\,s_Y^B(B) + \cos(\varphi)[s_X^A(A)\,s_X^B(B) + s_Z^A(A)\,s_Z^B(B)] - \sin(\varphi)[s_X^A(A)\,s_Z^B(B) - s_Z^A(A)\,s_X^B(B)]\} \quad (6)$$

Further we examine the case when the splittings due to the spin−orbit coupling and axial crystal field significantly exceed those caused by the exchange interaction. Under this condition

one can use the perturbation theory with the unperturbed Hamiltonian

$$H_0 = \sum_{i=A,B} \{-(3/2)\kappa\lambda \mathbf{l}_i \mathbf{s}_i + \Delta[l_{iZ}^2(i) - {}^2/_3]\} \quad (7)$$

and a perturbation

$$V = H_{ex} + \sum_{i=A,B} H_{ZE}^i \quad (8)$$

The Hamiltonian $H = H_0 + V$ operates within the total space $|j_A m_{jA}, j_B m_{jB}\rangle$, where j_A and j_B, as it was above-mentioned, take on the values $^1/_2$, $^3/_2$ and $^5/_2$. We have to pass from this Hamiltonian to the effective pseudo-spin-$^1/_2$ Hamiltonian that operates in the restricted space $|\Psi_{gr}^A(m_{jA}), \Psi_{gr}^B(m_{jB})\rangle$. Applying the second-order perturbation procedure for the degenerate level, one can present the effective pseudo-spin-$^1/_2$ Hamiltonian as follows:

$$H_{eff} = H_{eff}^{(1)} + H_{eff}^{(2)} \quad (9)$$

where $H_{eff}^{(1)}$ and $H_{eff}^{(2)}$ are the first- and second-order terms defined as

$$\langle \Psi_{gr}^A(m'_{jA}), \Psi_{gr}^B(m'_{jB}) | H_{eff}^{(1)} | \Psi_{gr}^A(m_{jA}), \Psi_{gr}^B(m_{jB}) \rangle = \langle \Psi_{gr}^A(m'_{jA}), \Psi_{gr}^B(m'_{jB}) | V | \Psi_{gr}^A(m_{jA}), \Psi_{gr}^B(m_{jB}) \rangle \quad (10)$$

and

$$\langle \Psi_{gr}^A(m'_{jA}), \Psi_{gr}^B(m'_{jB}) | H_{eff}^{(2)} | \Psi_{gr}^A(m_{jA}), \Psi_{gr}^B(m_{jB}) \rangle = -\sum_e \frac{\langle \Psi_{gr}^A(m'_{jA}), \Psi_{gr}^B(m'_{jB}) | V | e \rangle \langle e | V | \Psi_{gr}^A(m_{jA}), \Psi_{gr}^B(m_{jB}) \rangle^*}{E_e - E_0} \quad (11)$$

where E_0 and E_e are the ground and excited eigenvalues of H_0 and $|e\rangle$ represents the excited states of the Co(II) pair.

By calculating the matrix H_{eff} with the aid of eqs 10 and 11 and expressing it in terms of the standard spin-$^1/_2$ matrices $\tau_X^i(i)$, $\tau_Y^i(i)$, $\tau_Z^i(i)$, we arrive at the following final expression for the effective pseudo-spin-$^1/_2$ Hamiltonian:

$$H_{eff} = -2\tilde{J}_{XX}\tau_X^A(A)\,\tau_X^B(B) - 2\tilde{J}_{YY}\tau_Y^A(A)\,\tau_Y^B(B) - 2\tilde{J}_{ZZ}\tau_Z^A(A)\,\tau_Z^B(B) - 2\tilde{J}_{XZ}\tau_X^A(A)\,\tau_Z^B(B) - 2\tilde{J}_{ZX}\tau_Z^A(A)\,\tau_X^B(B) + \beta \sum_{i=A,B} \{\tilde{g}_{XX}\tau_X^i(i)\,H_X(i) + \tilde{g}_{YY}\tau_Y^i(i)\,H_Y(i) + \tilde{g}_{ZZ}\tau_Z^i(i)\,H_Z(i) + \tilde{g}_{XZ}[\tau_X^i(i)\,H_Z(i) + \tau_Z^i(i)\,H_X(i)] + \tilde{\Lambda}_{||}H_Z^2(i) + \tilde{\Lambda}_{\perp}[H_X^2(i) + H_Y^2(i)]\} \quad (12)$$

where the symbol i in the parenthesis indicates that the spin matrices as well as the magnetic field components refer to the local i-frames. The effective exchange integrals $\tilde{J}_{\alpha\beta}$, and the components of the effective g-tensor $\tilde{g}_{\alpha\beta}$ as well as the tensor of the temperature-independent paramagnetism (TIP) and $\tilde{\Lambda}_{||} = \tilde{\Lambda}_{ZZ}$ and $\tilde{\Lambda}_{\perp} = \Lambda_{XX} = \tilde{\Lambda}_{YY}$ are the known functions of the intrinsic microscopic parameters Δ, κ, λ and J. Because the components of the local g-tensors and TIP are the same for the ions A and B, we set in eq 12 $\tilde{g}_{\alpha\beta}^i \equiv \tilde{g}_{\alpha\beta}$, $\tilde{\Lambda}_{||}^i = \tilde{\Lambda}_{||}$, $\tilde{\Lambda}_{\perp}^i = \tilde{\Lambda}_{\perp}$. The Hamiltonian eq 12 differs in two main ways from that obtained in the framework of the phenomenological approach. First, eq 12 contains fewer nonzero parameters than the phenomenological one because the parameters $\tilde{J}_{XY}$, $\tilde{J}_{YX}$, $\tilde{J}_{YZ}$, $\tilde{J}_{ZY}$, $\tilde{g}_{XY}$, $\tilde{g}_{YX}$, $\tilde{g}_{YZ}$, $\tilde{g}_{ZY}$ prove to be vanishing. Second, the present microscopic approach provides the dependence of all nonvanishing parameters on the set of microscopic parameters.

To pass to the Hamiltonian defined in the molecular frame, we apply the transformation for the components of the magnetic field (eq A2 in Appendix) and the transformation reverse to that in eq A1 for the spin operators.

Then the effective Hamiltonian takes on the form

$$\hat{H}_{eff} = -2J_{XX}\tau_X^A\tau_X^B - 2J_{YY}\tau_Y^A\tau_Y^B - 2J_{ZZ}\tau_Z^A\tau_Z^B - 2J_{XZ}\tau_X^A\tau_Z^B - 2J_{ZX}\tau_Z^A\tau_X^B + \beta \sum_{i=A,B} \{g_{XX}^i\tau_X^i H_X + g_{YY}^i\tau_Y^i H_Y + g_{ZZ}^i\tau_Z^i H_Z + g_{XZ}^i(\tau_X^i H_Z + \tau_Z^i H_X)] + \Lambda_{XX}H_X^2 + \Lambda_{YY}H_Y^2 + \Lambda_{ZZ}H_Z^2 \quad (13)$$

In eq 13 all operators and components of the magnetic field are defined in the molecular frame. The parameters $J_{\alpha\beta}$ of the effective Hamiltonian defined in the molecular co-ordinates are connected to the parameters $\tilde{J}_{\alpha\beta}$ (local frames of reference) by the relations:

$$J_{XX} = \tilde{J}_{XX}\cos^2(\varphi/2) - \tilde{J}_{ZZ}\sin^2(\varphi/2) - \frac{1}{2}(\tilde{J}_{XZ} - \tilde{J}_{ZX})\sin(\varphi)$$

$$J_{YY} = \tilde{J}_{YY}$$

$$J_{ZZ} = -\tilde{J}_{XX}\sin^2(\varphi/2) + \tilde{J}_{ZZ}\cos^2(\varphi/2) - \frac{1}{2}(\tilde{J}_{XZ} - \tilde{J}_{ZX})\sin(\varphi)$$

$$J_{XZ} = \frac{1}{2}(\tilde{J}_{XX} + \tilde{J}_{ZZ})\sin(\varphi) + \tilde{J}_{XZ}\cos^2(\varphi/2) + \tilde{J}_{ZX}\sin^2(\varphi/2)$$

$$J_{ZX} = -\frac{1}{2}(\tilde{J}_{XX} + \tilde{J}_{ZZ})\sin(\varphi) + \tilde{J}_{XZ}\sin^2(\varphi/2) + \tilde{J}_{ZX}\cos^2(\varphi/2) \quad (14)$$

Similarly, the components of g-tensor $g_{\alpha\beta}^i$ are related to the components $\tilde{g}_{\alpha\beta}^i$ as follows:

$$g_{XX}^A = g_{YY}^B = \tilde{g}_{ZZ}\sin^2(\varphi/2) + \tilde{g}_{XX}\cos^2(\varphi/2) + \tilde{g}_{XZ}\sin(\varphi)$$

$$g_{YY}^A = g_{YY}^B = \tilde{g}_{YY}$$

$$g_{ZZ}^A = g_{ZZ}^B = \tilde{g}_{XX}\sin^2(\varphi/2) + \tilde{g}_{ZZ}\cos^2(\varphi/2) - \tilde{g}_{XZ}\sin(\varphi)$$

$$g_{XZ}^A = -g_{XZ}^B = \frac{1}{2}\sin(\varphi)(\tilde{g}_{ZZ} - \tilde{g}_{XX}) + \tilde{g}_{XZ}\cos(\varphi) \quad (15)$$

Finally, the relation between the components of the TIP-tensor $\Lambda_{\alpha\beta}$ and the components $\tilde{\Lambda}_{||}$ and $\tilde{\Lambda}_{\perp}$ is the following:

$$\Lambda_{XX} = 2[\tilde{\Lambda}_{||}\sin^2(\varphi/2) + \Lambda_{\perp}\cos^2(\varphi/2)]$$

$$\Lambda_{YY} = 2\tilde{\Lambda}_{\perp}$$

$$\Lambda_{ZZ} = 2[\tilde{\Lambda}_{\perp}\sin^2(\varphi/2) + \tilde{\Lambda}_{||}\cos^2(\varphi/2)] \quad (16)$$

The dependence of the exchange parameters $J_{\alpha\beta}$ on the axial field parameter Δ calculated for $J = -1.5$ and -2.5 cm^{-1} is shown in Figure 6. For the angle φ we used the value $\varphi = 54.6°$ that was determined from the geometrical structure of the cobalt(II) disphosphonate compound $Co(H_2L)(H_2O)$. From Figure 6 it is seen that $J_{XZ} = -J_{ZX}$, and that the degree of the exchange anisotropy depends on the strength of the axial crystal field. The differences between the parameters J_{XX}, J_{YY} and J_{ZZ} are more pronounced for negative Δ values. In the range -3000 cm$^{-1} < \Delta < -500$ cm^{-1} the parameter J_{ZZ} significantly exceeds in magnitude all other components of the $J_{\alpha\beta}$ tensor, and thus,

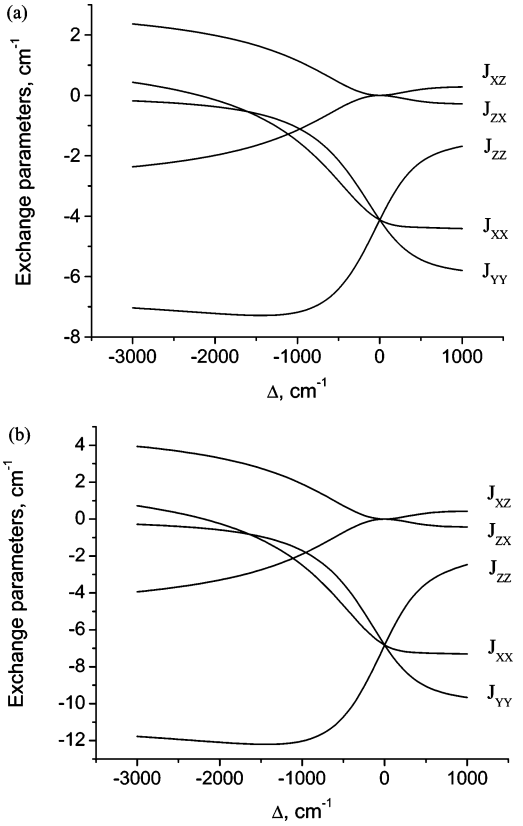

Figure 6. Exchange parameters J_{XZ}, J_{ZX}, J_{XX}, J_{YY}, J_{ZZ} as functions of the parameter Δ for $\kappa = 0.8$, $\lambda = -160$ cm^{-1}, $\varphi = 54.6°$, and $J = -1.5$ cm^{-1} (a) and $J = -2.5$ cm^{-1} (b).

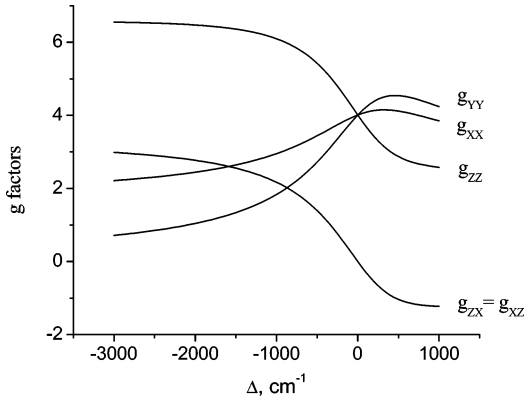

Figure 7. Dependence of the components $g^{A}_{\alpha\alpha} = g^{B}_{\alpha\alpha} = g_{\alpha\alpha}$ (α = *X*, *Y*, *Z*) and $g^{A}_{ZX} = g^{A}_{XZ} = -g^{B}_{ZX} = -g^{B}_{XZ} = g_{ZX} = g_{XZ}$ of the *g*-tensor on the parameter Δ calculated with $\kappa = 0.8$, $\lambda = -160$ cm^{-1}, $\varphi = 54.6°$, and $J = 1.5$ cm^{-1}.

the exchange Hamiltonian becomes highly anisotropic and approximately acquires the Ising form. At the same time the magnitudes of the parameters $J_{\alpha\beta}$ increase with the increase of the parameter $|J|$ of antiferromagnetic exchange. Finally, in the high-symmetry case, when the Co(II) ions are in the perfect octahedral surroundings (Δ = 0), the exchange Hamiltonian becomes isotropic $J_{XZ} = J_{ZX} = 0$, $J_{XX} = J_{YY} = J_{ZZ}$.

The dependence of the components of *g*-tensor $g^{A}_{\alpha\beta} = g^{B}_{\alpha\beta}$ on the parameter Δ calculated with $\kappa = 0.8$, $\lambda = -160$ cm^{-1}, $\varphi = 54.6°$ and $J = -1.5$ cm^{-1} is shown in Figure 7. In the case of Δ = 0 we obtain the well-known limits $g^{i}_{ZZ} = g^{i}_{XX} = g^{i}_{YY} = {}^{1}/_{2}(5g_e + 3\kappa)$, $g^{i}_{XZ} = 0$ that correspond to the fully isotropic Co(II) ion. The change in the magnitude and sign of the

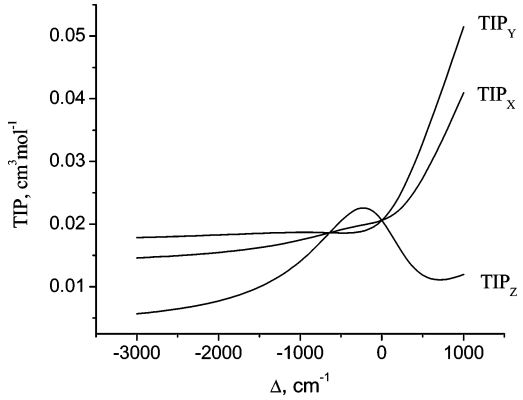

Figure 8. Components $TIP_\alpha = -2N_A\Lambda_{\alpha\alpha}$ (α = *X*, *Y*, *Z*) of the TIP tensor as functions of the parameter Δ: $\kappa = 0.8$, $\lambda = -160$ cm^{-1}, $\varphi = 54.6°$.

parameter Δ dramatically changes the components of the *g*-tensor. The most anisotropic case takes place for large negative values of Δ. At the same time for Δ < 0, the decrease of the Δ magnitude leads to the leveling of the *g*-factor values. Finally, Figure 8 illustrates the dependence of the components of the TIP tensor on the parameter Δ.

3. Mean Field Approximation. Evaluation of the Barrier for Magnetization Reversal

We start with the examination of the relaxation characteristics of the Co chain in the mean field approximation. The Hamiltonian of interacting Co ions in an infinite 1D chain with spin canting can be presented as

$$H = H_{\text{int}} + H_{\text{ZE}} \tag{17}$$

where H_{int} is the effective exchange Hamiltonian for the infinite chain and H_{ZE} describes the interaction of the A and B type Co ions in the chain with the external magnetic field. In the molecular coordinates, the Hamiltonian H_{int} of the chain in which A and B type ions alternate appears as follows:

$$H_{\text{int}} = -2\sum_{l}[J^{AB}_{XX}(\tau^{A}_{Xl}\tau^{B}_{l} + \tau^{B}_{Xl}\tau^{A}_{Xl+1}) + J^{AB}_{YY}(\tau^{A}_{Yl}\tau^{B}_{Yl} + \tau^{B}_{Yl}\tau^{A}_{Yl+1}) + J^{AB}_{ZZ}(\tau^{A}_{Zl}\tau^{B}_{Zl} + \tau^{B}_{Zl}\tau^{A}_{Zl+1}) + J^{AB}_{XZ}(\tau^{A}_{Xl}\tau^{B}_{Zl} - \tau^{B}_{Xl}\tau^{A}_{Zl+1} - \tau^{A}_{Zl}\tau^{B}_{Xl} + \tau^{B}_{Zl}\tau^{A}_{Xl+1})] \tag{18}$$

where *l* numbers the cells of the infinite chain, which contain an AB pair of Co ions. As eq 18 is written down, the following relations $J^{AB}_{\alpha\alpha} = J^{BA}_{aa}$ (α = *X*, *Y*, *Z*), $J^{AB}_{XZ} = -J^{BA}_{XZ}$, $J^{AB}_{ZX} = -J^{BA}_{ZX}$, $J^{AB}_{ZX} = -J^{AB}_{XZ}$ between the exchange parameters have been taken into account. One can derive these relations with the aid of eqs 6 and 12.

The Zeeman part of the chain Hamiltonian takes the form

$$\mathbf{H}_{\text{ZE}} = \sum_{l}\sum_{i=A,B}\beta[g^{i}_{XX}\tau^{i}_{Xl}H_X + g^{i}_{YY}\tau^{i}_{Yl}H_Y + g^{i}_{ZZ}\tau^{i}_{Zl}H_Z + g^{i}_{XZ}(\tau^{i}_{Xl}H_Z + \tau^{i}_{Zl}H_X)] \tag{19}$$

Passing to the molecular field approximation, we perform in eq 18 the following substitution:

$$\tau^{A}_{\alpha_l}\tau^{B}_{\beta_{l'}} = \bar{\tau}^{A}_{\alpha}\tau^{B}_{\beta_{l'}} + \tau^{A}_{\alpha_l}\bar{\tau}^{B}_{\beta} - \bar{\tau}^{A}_{\alpha}\bar{\tau}^{B}_{\beta} \qquad \alpha, \beta = X, Y, Z$$

where the parameters $\bar{\tau}^{A}_{\alpha}$ and $\bar{\tau}^{B}_{\beta}$ characterize the mean spins of

A and B ions and play the role of dimensionless order parameters

$$\bar{\tau}_\alpha^{\mathrm{A}} = \frac{\mathrm{Tr}[\exp(-\tilde{H}/kT)\tau_{\alpha_i}^{\mathrm{A}}]}{\mathrm{Tr}[\exp(-\tilde{H}/kT)]} \qquad \bar{\tau}_\beta^{\mathrm{B}} = \frac{\mathrm{Tr}[\exp(-\tilde{H}/kT)\tau_{\beta_i'}^{\mathrm{B}}]}{\mathrm{Tr}[\exp(-\tilde{H}/kT)]} \quad (20)$$

where $\tilde{H}$ is the chain Hamiltonian in the mean field approximation that decomposes into the sum of single ion Hamiltonians

$$\tilde{H} = \sum_n H_n^{\mathrm{A}} + \sum_m H_m^{\mathrm{B}} + 4N(J_{XX}^{\mathrm{AB}}\bar{\tau}_X^{\mathrm{A}}\bar{\tau}_X^{\mathrm{B}} - J_{XZ}^{\mathrm{AB}}\bar{\tau}_Z^{\mathrm{A}}\bar{\tau}_X^{\mathrm{B}} + J_{YY}^{\mathrm{AB}}\bar{\tau}_Y^{\mathrm{A}}\bar{\tau}_Y^{\mathrm{B}} + J_{XZ}^{\mathrm{AB}}\bar{\tau}_X^{\mathrm{A}}\bar{\tau}_Z^{\mathrm{B}} + J_{ZZ}^{\mathrm{AB}}\bar{\tau}_Z^{\mathrm{A}}\bar{\tau}_Z^{\mathrm{B}}) \quad (21)$$

Here N is the number of the AB cells in the chain, the indexes n and m label the ions of the sublattices A and B, respectively,

$$H_n^{\mathrm{A}} = (g_{XX}^{\mathrm{A}}H_X + g_{XZ}^{\mathrm{A}}H_Z - 4J_{XX}^{\mathrm{AB}}\bar{\tau}_X^{\mathrm{B}} - 4J_{XZ}^{\mathrm{AB}}\bar{\tau}_Z^{\mathrm{B}})\tau_{Xn}^{\mathrm{A}} + (g_{YY}^{\mathrm{A}}H_Y - 4J_{YY}^{\mathrm{AB}}\bar{\tau}_Y^{\mathrm{B}})\tau_{Yn}^{\mathrm{A}} + (g_{ZZ}^{\mathrm{A}}H_Z + g_{XZ}^{\mathrm{A}}H_X + 4J_{XZ}^{\mathrm{AB}}\bar{\tau}_X^{\mathrm{B}} - 4J_{ZZ}^{\mathrm{AB}}\bar{\tau}_Z^{\mathrm{B}})\tau_{Zn}^{\mathrm{A}} \quad (22)$$

$$H_m^{\mathrm{B}} = (g_{XX}^{\mathrm{B}}H_X + g_{XZ}^{\mathrm{B}}H_Z - 4J_{XX}^{\mathrm{AB}}\bar{\tau}_X^{\mathrm{A}} + 4J_{XZ}^{\mathrm{AB}}\bar{\tau}_Z^{\mathrm{A}})\tau_{Xm}^{\mathrm{B}} + (g_{YY}^{\mathrm{B}}H_Y - 4J_{YY}^{\mathrm{AB}}\bar{\tau}_Y^{\mathrm{A}})\tau_{Ym}^{\mathrm{A}} + (g_{ZZ}^{\mathrm{B}}H_Z + g_{XZ}^{\mathrm{B}}H_X - 4J_{XZ}^{\mathrm{AB}}\bar{\tau}_X^{\mathrm{A}} - 4J_{ZZ}^{\mathrm{AB}}\bar{\tau}_Z^{\mathrm{A}})\tau_{Zm}^{\mathrm{B}} \quad (23)$$

The eigenvalues of the Hamiltonian eqs 22 and 23 depend on the order parameters as well as on magnetic field components and appear as follows:

$$E_{1,2}^{\mathrm{A}} = \pm f^{\mathrm{A}}(H_X,H_Y,H_Z,\bar{\tau}_X^{\mathrm{B}},\bar{\tau}_Y^{\mathrm{B}},\bar{\tau}_Z^{\mathrm{B}})$$
$$E_{1,2}^{\mathrm{B}} = \pm f^{\mathrm{B}}(H_X,H_Y,H_Z,\bar{\tau}_X^{\mathrm{A}},\bar{\tau}_Y^{\mathrm{A}},\bar{\tau}_Z^{\mathrm{A}}) \quad (24)$$

Here the function $f^A(H_X, H_Y, H_Z, \bar{\tau}_X^{\mathrm{B}}, \bar{\tau}_Y^{\mathrm{B}}, \bar{\tau}_Z^{\mathrm{B}})$ takes the form

$$f^{\mathrm{A}}(H_X,H_Y,H_Z,\bar{\tau}_X^{\mathrm{B}},\bar{\tau}_Y^{\mathrm{B}},\bar{\tau}_Z^{\mathrm{B}}) = \Big[\frac{1}{4}((g_{XX}^{\mathrm{A}})^2 + (g_{XZ}^{\mathrm{A}})^2)H_X{}^2 + \frac{1}{4}(g_{YY}^{\mathrm{A}})^2H_Y{}^2 + \frac{1}{4}((g_{XZ}^{\mathrm{A}})^2 + (g_{ZZ}^{\mathrm{A}})^2)H_Z{}^2 - \frac{1}{2}(g_{XX}^{\mathrm{A}} + g_{ZZ}^{\mathrm{A}})g_{XZ}^{\mathrm{A}}H_XH_Z - 2(g_{XX}^{\mathrm{A}}J_{XX}^{\mathrm{AB}} + g_{XZ}^{\mathrm{A}}J_{XZ}^{\mathrm{AB}})H_X\bar{\tau}_X^{\mathrm{B}} + 2(g_{XZ}^{\mathrm{A}}J_{XX}^{\mathrm{AB}} + g_{ZZ}^{\mathrm{A}}J_{XZ}^{\mathrm{AB}})H_Z\bar{\tau}_X^{\mathrm{B}} - 2g_{YY}^{\mathrm{A}}J_{YY}^{\mathrm{AB}}H_Y\bar{\tau}_Y^{\mathrm{B}} + 2(g_{XZ}^{\mathrm{A}}J_{ZZ}^{\mathrm{AB}} - g_{XX}^{\mathrm{A}}J_{XZ}^{\mathrm{AB}})H_X\bar{\tau}_Z^{\mathrm{B}} + 2(g_{XZ}^{\mathrm{A}}J_{XZ}^{\mathrm{AB}} - g_{ZZ}^{\mathrm{A}}J_{ZZ}^{\mathrm{AB}})H_Z\bar{\tau}_Z^{\mathrm{B}} + 8(J_{XX}^{\mathrm{AB}}J_{XZ}^{\mathrm{AB}} - J_{XZ}^{\mathrm{AB}}J_{ZZ}^{\mathrm{AB}})\bar{\tau}_X^{\mathrm{B}}\bar{\tau}_Z^{\mathrm{B}} + 4(J_{XX}^{\mathrm{AB}})^2(\bar{\tau}_X^{\mathrm{B}})^2 + 4(J_{XZ}^{\mathrm{AB}})^2(\bar{\tau}_X^{\mathrm{B}})^2 + 4(J_{YY}^{\mathrm{AB}})^2(\bar{\tau}_Y^{\mathrm{B}})^2 + 4(J_{XZ}^{\mathrm{AB}})^2(\bar{\tau}_Z^{\mathrm{B}})^2 + 4(J_{ZZ}^{\mathrm{AB}})^2(\bar{\tau}_Z^{\mathrm{B}})^2\Big]^{1/2} \quad (25)$$

The function $f^B(H_X, H_Y, H_Z, \bar{\tau}_X^{\mathrm{A}}, \bar{\tau}_Y^{\mathrm{A}}, \bar{\tau}_Z^{\mathrm{A}})$ can be obtained from eq 25 by means of the substitution $\bar{\tau}_\alpha^{\mathrm{B}} \rightarrow \bar{\tau}_\alpha^{\mathrm{A}}$ ($\alpha = X, Y, Z$). The free energy of the AB unit cell can be expressed as

$$F = -kT\ln[2\cosh(f^{\mathrm{A}}(H_X,H_Y,H_Z,\bar{\tau}_X^{\mathrm{B}},\bar{\tau}_Y^{\mathrm{B}},\bar{\tau}_Z^{\mathrm{B}}))] - kT\ln[2\cosh(f^{\mathrm{B}}(H_X,H_Y,H_Z,\bar{\tau}_X^{\mathrm{A}},\bar{\tau}_Y^{\mathrm{A}},\bar{\tau}_Z^{\mathrm{A}}))] + 4(J_{XX}^{\mathrm{AB}}\bar{\tau}_X^{\mathrm{A}}\bar{\tau}_X^{\mathrm{B}} + J_{YY}^{\mathrm{AB}}\bar{\tau}_Y^{\mathrm{A}}\bar{\tau}_Y^{\mathrm{B}} + J_{ZZ}^{\mathrm{AB}}\bar{\tau}_Z^{\mathrm{A}}\bar{\tau}_Z^{\mathrm{B}} + J_{XZ}^{\mathrm{AB}}\bar{\tau}_X^{\mathrm{A}}\bar{\tau}_Z^{\mathrm{B}} - J_{XZ}^{\mathrm{AB}}\bar{\tau}_Z^{\mathrm{A}}\bar{\tau}_X^{\mathrm{B}}) \quad (26)$$

The order parameters $\bar{\tau}_X^{\mathrm{A}}$, $\bar{\tau}_Y^{\mathrm{A}}$, $\bar{\tau}_Z^{\mathrm{A}}$, $\bar{\tau}_X^{\mathrm{B}}$, $\bar{\tau}_Y^{\mathrm{B}}$, $\bar{\tau}_Z^{\mathrm{B}}$ can be obtained by the numerical solution of the set of self-consistent equations

$$\left(\frac{\partial F}{\partial\bar{\tau}_X^{\mathrm{A}}}\right) = 0, \left(\frac{\partial F}{\partial\bar{\tau}_Y^{\mathrm{A}}}\right) = 0, \left(\frac{\partial F}{\partial\bar{\tau}_Z^{\mathrm{A}}}\right) = 0,$$
$$\left(\frac{\partial F}{\partial\bar{\tau}_X^{\mathrm{B}}}\right) = 0, \left(\frac{\partial F}{\partial\bar{\tau}_Y^{\mathrm{B}}}\right) = 0, \left(\frac{\partial F}{\partial\bar{\tau}_Z^{\mathrm{B}}}\right) = 0 \quad (27)$$

Equations 27 are not explicitly listed here due to their hugeness.

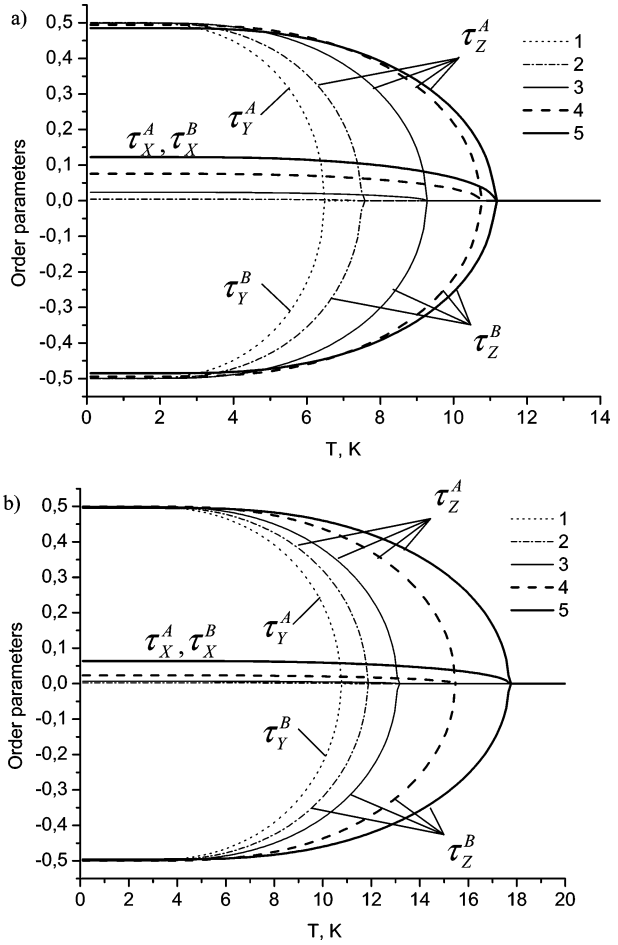

Figure 9. Order parameters as functions of the axial distortion Δ in the case of $\kappa = 0.8$, $\lambda = -160$ cm^{-1}. (a) $J = -1.5$ cm^{-1} and $\Delta = 100$ cm^{-1} (doted line), $T_C = 6.4$ K (1); $\Delta = -200$ cm^{-1} (dot-dashed line), $T_C = 7.5$ K (2); $\Delta = -500$ cm^{-1} (solid line), $T_C = 9.2$ K (3); $\Delta = -1150$ cm^{-1} (thick dashed line), $T_C = 10.7$ K (4); $\Delta = -2000$ cm^{-1} (thick solid line), $T_C = 11.1$ K (5). (b) $J = -2.5$ cm^{-1} and $\Delta = 100$ cm^{-1} (doted line), $T_C = 10.7$ K (1); $\Delta = -150$ cm^{-1} (dot-dashed line), $T_C = 11.9$ K (2); $\Delta = -250$ cm^{-1} (solid line), $T_C = 13.1$ K (3); $\Delta = -500$ cm^{-1} (thick dashed line), $T_C = 15.5$ K (4); $\Delta = -1000$ cm^{-1} (thick solid line), $T_C = 17.7$ K (5).

The procedure of calculation of the temperature dependence of the order parameters with the aid of eq 27 was carried out in two stages. First, we calculate the parameters of the effective exchange Hamiltonian, the g and TIP tensors for ions A and B as functions of the axial distortion Δ, and then we numerically solve the system of eqs 27.

We start with an inspection of the influence of the parameter Δ describing the axial splitting of the $^4T_1$ term of the Co(II) ion on the type of spin ordering. The corresponding parameters of the effective exchange Hamiltonian necessary for calculations of the mean spin values can be easily obtained with the aid of Figure 6. In Figure 9 the effective spin components $\bar{\tau}_\alpha^{\mathrm{A}}$ and $\bar{\tau}_\alpha^{\mathrm{B}}$ are depicted for different Δ and J ($J < 0$) values. It is seen that, in the case of relatively strong negative axial field ($\Delta < 0$), the Z-components $\bar{\tau}_Z^{\mathrm{A}}$ and $\bar{\tau}_Z^{\mathrm{B}}$ line up antiparallel, and the Y-components vanish. At the same time, until the critical value value Δ_{cr} ($\Delta < 0$) is reached, the X-components are nonvanishing and parallel $\bar{\tau}_X^{\mathrm{A}} = \bar{\tau}_X^{\mathrm{B}}$. Such an uncompensated magnetic moment appears in the case of sufficiently large negative local distortions that lead to the inequalities $|J_{ZZ}|, |J_{XZ}| > |J_{XX}|, |J_{YY}|$ and $|J_{ZZ}| > |J_{XZ}|$ between the parameters of the effective exchange Hamiltonian. The increase of the absolute value of Δ ($\Delta < 0$) leads both to the increase of the temperature

of the phase transition and the magnitude of the *X*-components of the effective spin (Figure 9). We thus arrive at the conclusion that even the antiferromagnetic exchange interaction is able to produce a ferromagnetic type spin alignment along the *X*-axis. Such an unusual effect is obviously the consequence of the spin canting in the chain and significant local axial anisotropy of a negative sign. Note that in the adopted pseudo-spin-$^1/_2$ formalism the term "spin canting" relates to the effective spins of the ground Kramers doublets rather than to the true spins $S = {}^3/_2$ of the Co(II) ions.

For $\Delta > \Delta_{cr}$ an alternative qualitative picture arises (Figure 9). In this case the accumulation of the magnetic moment along the *X*-axis does not occur, and only an antiferromagnetic type ordering takes place. Providing $\Delta_{cr} < \Delta < 0$ the magnetic moments $\bar{\tau}_Z^A = -\bar{\tau}_Z^B$ are aligned along the *Z*-axis, and for $\Delta > 0$ they turn around and become oriented along the *Y*-axis ($\bar{\tau}_Y^A = -\bar{\tau}_Y^B$). Such a reorientation of the spins can be explained by the behavior of the exchange parameters as functions of Δ. As a matter of fact, for $\Delta_{cr} < \Delta < 0$ the exchange parameter $|J_{ZZ}|$ exceeds the parameters $|J_{XX}|$, $|J_{YY}|$, $|J_{XZ}|$ whereas for $\Delta > 0$ the relation $|J_{YY}| > |J_{XX}|$, $|J_{ZZ}|$, $|J_{XZ}|$ holds (Figure 6).

Now let us analyze the composition of the wavefunctions corresponding to the energy levels $E_{1,2}^A$ and $E_{1,2}^B$ of ions A and B in the molecular field for negative values of the parameter Δ satisfying the inequality $\Delta < \Delta_{cr}$. Numerical calculations show that in the absence of an external magnetic field these wavefunctions can be written down in the form

$$\psi_{1,2}^A = \pm c_1|\pm {}^1/_2\rangle + c_2|\mp {}^1/_2\rangle \qquad \psi_{1,2}^B = c_2|\pm {}^1/_2\rangle \pm c_1|\mp {}^1/_2\rangle \tag{28}$$

where the coefficients c_1 and c_2 satisfy the inequality $|c_2|^2 >> |c_1|^2$. For instance, for $\Delta = -500$ cm^{-1}, $J = -1.5$ cm^{-1} and $T < 9.1$ *K* one obtains $|c_2|^2 = 0.9994$, $|c_1|^2 = 0.0006$. Thus, the excited and the ground states of A-type ions mainly correspond to the pseudo-spin projections $-^1/_2$ and $+^1/_2$, respectively. For B-type ions a reverse order of levels takes place. This means that for both types of ions in the chain the transition from the ground state to the excited one is accompanied by a spin flip. Thus, to change the sign of the spin projection of an ion in the molecular field induced by the chain, a barrier of the magnitude $U = E_1^A - E_2^A = E_1^B - E_2^B$ must be overcome. The magnitude of this barrier is obviously determined by the parameters λ, Δ and *J*, which describe the key intra- and intercenter interactions in the chain. At the same time *U* can be regarded as a reasonable measure of the barrier energy only for $\Delta < \Delta_{cr}$ when an uncompensated magnetic moment exists. Actually, *U* represents the energy that should be applied to the system to destroy the ferromagnetic type spin alignment along the *X* axis. Figure 10 illustrates the dependence of the barrier magnitude *U* on the parameter Δ for $\kappa = 0.8$, $\lambda = -160$ cm^{-1}, $J = -1.5$ cm^{-1} and $\varphi = 54.6°$. It can be seen that the barrier magnitude *U* represents a nonmonotonic function of the parameter Δ. With the decrease of the magnitude of Δ, the *U* value increases, passes through a maximum and then decreases monotonically. For $\Delta = -1147$ cm^{-1} the barrier reaches the maximum value $U_{max} = 14.3$ cm^{-1}. Insofar as the order parameters (Figure 9a) and, thus, the energy levels, eq 24 keep their constant values over a comparatively wide temperature range, the barrier height also remains constant in this range. However, the decrease of the order parameters with temperature leads to the diminution of the energy barrier to reverse the magnetization direction. Simple analysis of Figures 6a and 9 also shows that in the range $|\Delta_{cr}| < |\Delta| < 3000$ cm^{-1}, the barrier height can be evaluated as $U \approx 2J_{ZZ}$,

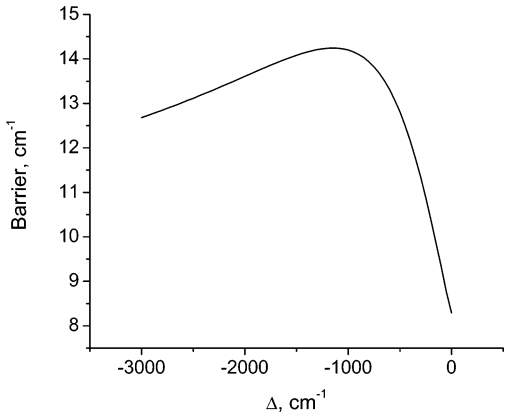

Figure 10. Variation of the barrier for magnetization reversal as a function of negative axial distortions Δ with $\kappa = 0.8$, $\lambda = -160$ cm^{-1}, $J = -1.5$ cm^{-1}, $\varphi = 54.6°$.

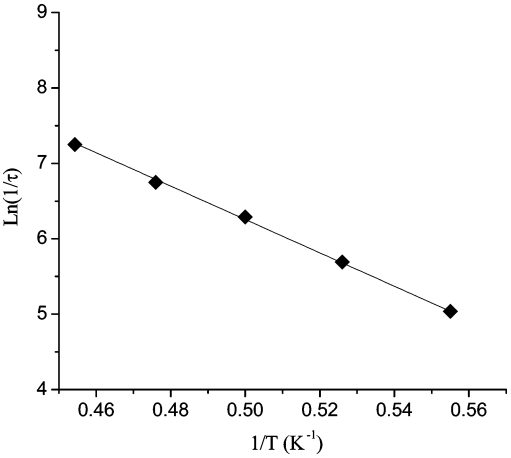

Figure 11. Temperature dependence of the relaxation time. The squares represent the calculated experimental values,[26] the solid line corresponds to the best fit of the data to eq 30.

and hence in this particular case we arrive at the Glauber's result[20] obtained in the framework of the 1D Ising model. Actually, for $|\Delta_{cr}| < |\Delta| < 3000$ cm^{-1} (Figure 6a), the parameters of the effective exchange Hamiltonian eq 13 are subjected to the inequality $|J_{ZZ}| >> |J_{XX}|$, $|J_{YY}|$, $|J_{XZ}|$, so that the effective Hamiltonian takes on the Ising form:

$$H_{eff} = -2J_{ZZ}\tau_Z^A\tau_Z^B \tag{29}$$

In this case, according to the Glauber theory, the magnitude of the barrier for spin reorientation is shown to correspond to the energy loss in the one-spin flip-flop process; that is, it is approximately equal to $8J_{ZZ}({}^1/_2)^2 = 2J_{ZZ}$.

Finally, we determine the axial distortion Δ of the local surrounding of Co(II) ions in the $Co(H_2L)(H_2O)$ compound using the experimental data on the temperature dependence of the relaxation time in this compound and the calculated dependence of the parameters $J_{\alpha\beta}$ and *U* on Δ (Figure 10). The temperature dependence of the relaxation time was obtained from the frequency dependence of the components χ' and χ'' of the *ac* susceptibility (Figure 3) and it is presented in Figure 11. The experimental data for τ were fit to the Arrhenius expression

$$\tau(T) = \tau_0 \exp\left(\frac{U}{kT}\right) \tag{30}$$

The best fit parameters were found to be $U = 15.4$ cm^{-1}, $\tau_0 =$

3×10^{-8} s. Comparing these values with the calculated dependence of the barrier height on the parameter Δ, we find that the barrier energy estimated from the experimental data is in satisfactory accord with that calculated for $\Delta = -1150$ cm^{-1}. To support the contention that the parameter values $\Delta = -1150$ cm^{-1} and $J = -1.5$ cm^{-1} are the only ones that conform to the observed magnitude of the barrier, we refer to Figures 6b and 9b. From Figure 9b it follows that for $J = -2.5$ cm^{-1} a nonvanishing magnetic moment directed along the X axis already appears for the value $\Delta = -500$ cm^{-1}, which corresponds to the barrier energy $U = 2J_{ZZ} \approx 21.4$ cm^{-1} (Figure 6b) that is higher than the observed one. From Figure 6b it is seen that for $|\Delta| > 500$ cm^{-1} and $J = -2.5$ cm^{-1} the barrier energy increases. For $|\Delta| < 500$ cm^{-1} an uncompensated magnetic moment cannot appear, the anisotropy of the effective exchange Hamiltonian diminishes, and the concept of the barrier becomes inapplicable. It is clear that in the case of antiferromagnetic exchange and $|J| < 1.5$ cm^{-1} for all favorable values of Δ the barrier energy will be noticeably lower than that extracted from the experimental data.

4. Magnetic Properties

In the framework of the mean field approximation we were able to elucidate the conditions under which an uncompensated magnetic moment appears and to obtain a reasonable value for the axial field parameter providing the experimental barrier value. However, the known deficiencies of the mean field approximation in examination of the magnetic properties led us to simulate the magnetic behavior of an infinite chain by calculation of the properties of a closed ring chain with N unit cells each cell containing a pair of ions A and B. Extrapolation of these properties to the infinite N number gives us the behavior of the named infinite chain. In these calculations we use the energy levels obtained by exact solution of the quantum-mechanical problem for the ring chain using the value $\Delta = -1150$ cm^{-1} found in section 3. The diagonal components of the magnetic susceptibility are determined as

$$\chi_{\alpha\alpha} = N_A k_B T \frac{\partial^2}{\partial H_\alpha^2}[\ln Z(H_\alpha)]H_\alpha \rightarrow 0 \qquad (31)$$

The susceptibility of the powder sample is calculated with the aid of the expression:

$$\chi = \frac{1}{3}(\chi_{XX} + \chi_{YY} + \chi_{ZZ}) \qquad (32)$$

The calculations were performed for a chain containing up to 5 unit cells AB (10 spins). In this case the size of the Hamiltonian matrix is 1024. This number of cells is enough to demonstrate the main peculiarities of the magnetic properties. While deriving the effective exchange Hamiltonian, we restricted our consideration to the lowest Kramers doublets of ions A and B. For this reason we consider only the magnetic properties at temperatures lower than 50 K.

Figure 12 presents the magnetic susceptibility of a ring chain consisting of 10 Co ions ($N = 5$) as a function of the exchange parameter J. One can see that with a temperature decrease the magnetic susceptibility diminishes, then passes through a minimum, and finally increases. The position of the minimum shifts to the low-temperature range for smaller values of $|J|$. In such a way the parameters $J = -1.5$ cm^{-1} and $\Delta = -1150$ cm^{-1} not only fit the experimental value of the barrier energy

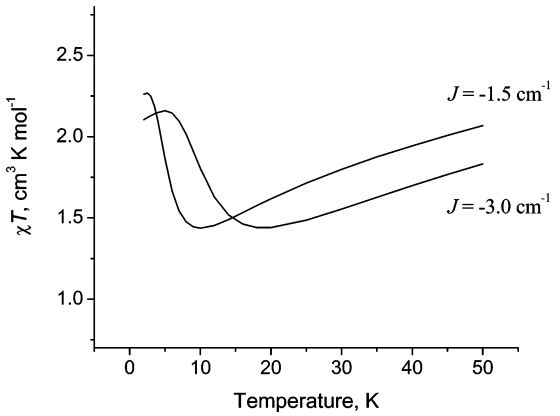

Figure 12. Temperature variation of the magnetic susceptibility of a ring chain with $N = 5$ unit cells for $\kappa = 0.8$, $\Delta = -1150$ cm^{-1}, $\lambda = -160$ cm^{-1}, $\varphi = 54.6°$, $J = -1.5$ and -3 cm^{-1}.

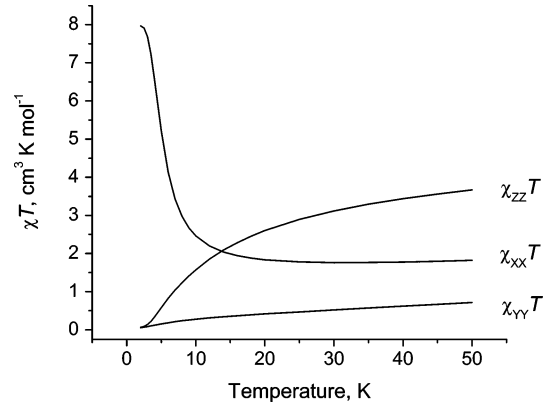

Figure 13. Diagonal components of the χT tensor as functions of temperature for $\kappa = 0.8$, $\Delta = -1150$ cm^{-1}, $\lambda = -160$ cm^{-1}, $\varphi = 54.6°$, $J = -1.5$ cm^{-1}, $N = 5$.

but also ensure the minimum of the χT curve at $T = 7$ K, which is in agreement with the experimental data (Figure 2). The increase of χT at low temperature is due to spin canting. This canting arises from the competition between the axial single ion anisotropy and the magnetic exchange interaction. It should be emphasized that the position of the curve maximum and its height are in satisfactory agreement with experimental data. However, the calculated χT value in the minimum is higher than that observed, and this is most likely related to our simplified model, which neglects the rhombic distortion of the local surroundings of the Co ions. At the same time for the parameters $J = -1.5$ cm^{-1} and $\Delta = -1150$ cm^{-1} the model well reproduces the main qualitative features of the observed magnetic behavior.

The temperature dependence of $\chi_{XX}T$, $\chi_{YY}T$ and $\chi_{ZZ}T$ is presented in Figure 13. It can be seen that, at low temperatures, the system exhibits strong magnetic anisotropy. Thus, at $T <$ 10 K, the $\chi_{XX}T$ component of the tensor χT significantly exceeds the components $\chi_{YY}T$ and $\chi_{ZZ}T$ and indicates the presence of an uncompensated magnetic moment directed along the molecular X axis. This behavior of the χT tensor components is in accord with the results obtained from the mean field approximation.

5. Concluding Remarks

The recently discovered SCM behavior of the cobalt(II) disphosphonate compound $Co(H_2L)(H_2O)$ based on spin canting

in a antiferromagnetically coupled Co(II) chain is the subject of this current study. The new theoretical model of this effect allows for the spin−orbit interaction, the axial component of the crystal field acting on the ground-state cubic $^4T_1$ terms of the Co(II) ions and the isotropic antiferromagnetic exchange interaction. The cornerstone of the model is the effect of spin canting that arises from the inclination of the local anisotropy axes with respect to each other.

The results obtained in the present paper can be summarized as follows. The effective pseudo-spin-$^1/_2$ exchange Hamiltonian operating within the ground Kramers doublets of two Co(II)-ions has been derived by taking into account the different orientation of the local coordinate axes of these ions. The dependence of the effective Hamiltonian parameters (components of the exchange, TIP and g tensors) on the initial local and intercenter microscopic parameters has been found. With the aid of this highly anisotropic Hamiltonian the SCM properties of the $Co(H_2L)(H_2O)$ compound have been examined in a combined approach comprising both the mean field approximation and the exact quantum-mechanical solution for a ring chain. In the framework of the mean field approximation for a definite range of negative local axial distortions, the possibility of appearance of an uncompensated magnetic moment is revealed in an infinite chain with spin canting and an antiferromagnetic Heisenberg exchange interaction. The height of the barrier for magnetization reversal has been calculated as a function of the value of the negative axial crystal field parameter. The magnitude of this parameter determining the barrier height for the titled compound has been estimated. The calculated temperature dependence of the magnetization relaxation time was found to be in satisfactory agreement with experimental data. We have also shown that the ring chain approach reasonably describes the experimental magnetic susceptibility curve for the set of microscopic parameters consistent with the observed barrier height.

To discuss the real 1D Co(II) chain in more detail, the adopted model needs to be generalized in several aspects. First, a more precise model of the local symmetry of the Co(II) ions in the chain should be introduced in conformity with X-ray data. Second, the suggested model is limited to the consideration of the lowest Kramers doublet of each Co(II) ion. This in its turn allows only the consideration of the low-temperature magnetic properties. A new computational approach to the problem of the magnetic properties of the 1D Co(II) chain that takes into account the whole energy patterns of the constituent ions and provides an opportunity to simulate the magnetic properties up to room temperature should be developed. The quantum-mechanical estimation of the parameter of exchange interaction and values of the local distortions would be also useful. In spite of these restricting assumptions in the treatment carried out in this work, the suggested model reflects the main qualitative features of the observed phenomenon. The developed approaches explain the SCM behavior of the $Co(H_2L)(H_2O)$ compound and represent the first attempt to exceed the limits of the usually accepted SCM model based on consideration of Heisenberg exchange and zero-field splitting Hamiltonians inapplicable for systems with unquenched orbital momenta.

Appendix

Transformation connecting the spin operator components in the molecular and local frames:

$$\begin{pmatrix} s_X^A \\ s_Y^A \\ s_Z^A \end{pmatrix} = \begin{pmatrix} \cos(\varphi/2) & 0 & \sin(\varphi/2) \\ 0 & 1 & 0 \\ -\sin(\varphi/2) & 0 & \cos(\varphi/2) \end{pmatrix} \begin{pmatrix} s_X^A(A) \\ s_Y^A(A) \\ s_Z^A(A) \end{pmatrix}$$

$$\begin{pmatrix} s_X^B \\ s_Y^B \\ s_Z^B \end{pmatrix} = \begin{pmatrix} \cos(\varphi/2) & 0 & -\sin(\varphi/2) \\ 0 & 1 & 0 \\ \sin(\varphi/2) & 0 & \cos(\varphi/2) \end{pmatrix} \begin{pmatrix} s_X^B(B) \\ s_Y^B(B) \\ s_Z^B(B) \end{pmatrix} \quad \text{(A1)}$$

Transformation connecting the magnetic field components in the molecular and local frames:

$$\begin{pmatrix} H_X(A) \\ H_Y(A) \\ H_Z(A) \end{pmatrix} = \begin{pmatrix} \cos(\varphi/2) & 0 & -\sin(\varphi/2) \\ 0 & 1 & 0 \\ \sin(\varphi/2) & 0 & \cos(\varphi/2) \end{pmatrix} \begin{pmatrix} H_X \\ H_Y \\ H_Z \end{pmatrix}$$

$$\begin{pmatrix} H_X(B) \\ H_Y(B) \\ H_Z(B) \end{pmatrix} = \begin{pmatrix} \cos(\varphi/2) & 0 & \sin(\varphi/2) \\ 0 & 1 & 0 \\ -\sin(\varphi/2) & 0 & \cos(\varphi/2) \end{pmatrix} \begin{pmatrix} H_X \\ H_Y \\ H_Z \end{pmatrix} \quad \text{(A2)}$$

Acknowledgment. The research described in this publication was made possible in part by Award No. MOC2-2611-CH-04 of the U.S. Civilian Research & Development Foundation for the Independent States of the Former Soviet Union (CRDF) and Award No. MTFP-04-01 Follow-On-Award of the Moldovan Research and Development Association (MRDA) and CRDF. Financial support of the Supreme Council for Science and Technological Development of Moldova is also appreciated. K.R.D. gratefully acknowledges the support of the Department of Energy (Grant DE-FG02-02ER45999).

References and Notes

(1) Gatteschi, D.; Sessoli, R. *Angew. Chem., Int. Ed.* **2003**, *42*, 269.
(2) Awschalom, D. D.; Di Vencenzo, D. P. *Phys. Today* **1995**, 43.
(3) Sessoli, R.; Tsai, H.-L.; Schake, A. R.; Wang, S.; Vincent, J. B.; Folting, K.; Gatteschi, D.;Christou, G.; Hendrickson, D. N. *J. Am. Chem. Soc.* **1993**, *115*, 1804.
(4) Sessoli, R.; Gatteschi, D.; Caneschi, A.; Novak, M. A. *Nature* **1993**, *365*, 141.
(5) Eppley, H. J.; Tsai, H.-L.; de Vries, N.; Folting, K.; Christou, G.; Hendrickson, D. N. *J. Am. Chem. Soc.* **1995**, *117*, 301.
(6) Aubin, S. M. J.; Sun, Z.; Pardi, L.; Krzystek, J.; Folting, K.; Brunel, L.-C.; Rheingold, A. L.; Christou, G.; Hendrickson, D. N. *Inorg. Chem.* **1999**, *38*, 5329.
(7) Soler, M.; Chandra, S. K.; Ruiz, D.; Davidson, E. R.; Hendrickson, D. N.; Christou, G. *Chem. Commun.* **2000**, 2417.
(8) Müller, A.; Luban, M.; Schröder, C.; Modler, R.; Kögerler, P.; Axenovich, M; Schnack, J.; Canfield, P.; Bud'ko, S.; Harrison, N. *Chem. Phys. Chem.* **2001**, *2*, 517.
(9) Tasiopoulos, A. J.; Vinslava, A.; Wernsdorfer, W.; Abboud, K. A.; Christou, G. *Angew. Chem., Int. Ed.* **2004**, *43*, 2117.
(10) Sokol, J. J.; Hee, A. G.; Long, J. R. *J. Am. Chem. Soc.* **2002**, *124*, 7656.
(11) Choi, H. J.; Sokol, J. J.; Long, J. R. *Inorg. Chem.* **2004**, *43*, 1606.
(12) Caneschi, A.; Gatteschi, D.; Lalioti, N.; Sangregorio, C.; Sessoli, R.; Venturi, G.; Vindigni, A.; Rettori, A.; Pini, M. G.;Novak, M. A. *Angew. Chem., Int. Ed.* **2001**, *40*, 1760.
(13) Caneschi, A.; Gatteschi, D.; Lalioti, N.; Sangregorio, C.; Sessoli, R.; Sorace, L.; Tangoulis, V.; Vindigni, A. *Chem. Eur. J.* **2002**, *8*, 286.
(14) Caneschi, A.; Gatteschi, D.; Lalioti, N.; Sangregorio, C.; Sessoli, R.;Venturi, G.;Vindigni, A.; Rettori, A.; Pini, M. G.; Novak, M. A. *Europhys. Lett.* **2002**, *58*, 771.
(15) Clerac, R; Miyasaka, H; Yamashita, M; Coulon, *C. J. Am. Chem. Soc.* **2002**, *124*, 12837.
(16) Lescouëzec, R.;Vaisserman, J.; Rui-Perez, C.; Lloret, F.; Carrasco, R.; Julve, M; Verdaquer, M.; Draomzee, D.; Gatteschi, D.; Wernsdorfer, W. *Angew. Chem.* **2003**, *115*,1521.
(17) Lescouëzec, R.;Vaisserman, J.; Rui-Perez, C.; Lloret, F.; Carrasco, R.; Julve, M; Verdaquer, M.; Draomzee, D.; Gatteschi, D.; Wernsdorfer, W. *Angew. Chem. Int. Ed.* **2003**, *42*, 1483.
(18) Miyasaka, H; Clerac, R; Mizushima, K; Sugiura, K; Yamashita, M; Wernsdorfer, W.; Coulon, C. *Inorg. Chem.* **2003**, *42*, 8203.

(19) Coulon, C.; Clerac, R.; Lecren, L.; Wernsdorfer, W.; Miyasaka, H. *Phys. Rev.* **2004**, *B69*, 132408.

(20) Glauber, R. J. *J. Math. Phys.* **1963**, *4*, 294.

(21) Berlinguette, C. P.; Vaughn, D.; Cañada-Vilalta, C.; Galán-Mascarós, J.-R.; Dunbar, K. R. *Angew. Chem. Int. Ed*. **2003**, *42*, 1523.

(22) Wang, S.; Zuo, J. L.; Zhou, H. C.; Choi, H. J.; Ke, Y.; Long, J. R. *Angew. Chem., Int. Ed.* **2004**, *43*, 5940.

(23) Palii, A. V.; Ostrovsky, S. M.; Klokishner, S. I.; Tsukerblat, B. S.; Galán-Mascarós, J. R.; Berlinguette, C. P.; Dunbar, K. R. *J. Am. Chem. Soc.* **2004**, *126*, 16860.

(24) Tsukerblat, B. S.; Palii, A. V.; Ostrovsky, S. M.; Kunitsky, S. V.; Klokishner, S. I.; Dunbar, K. R. *J. Chem. Theory Computation* **2005**, *1*, 668.

(25) Palii, A. V.; Ostrovsky, S. M.; Klokishner, S. I.; Tsukerblat, B. S.; Dunbar, K. R. *Chem. Phys. Chem.* **2006**, *7*, 871.

(26) Sun, Z.-M.; Prosvirin, A. V.; Zhao, H.-H.; Mao, J.-G.; Dunbar, K. R. *J. Appl. Phys.* **2005**, *97*, 10B305.

(27) Zhao, H.-H.; Prosvirin, A. V.; Galah-Mascaros, J. R.; Gomez-Garcia, C. J.; Dunbar, K. R. Mn(III) chain.

(28) Coronado, E.; Drillon, M.; Nugteren, P. R.; de Jongh, L. J.; Beltran, D. *J. Am. Chem. Soc.* **1988**, *110*, 3907.

(29) Clemente, J. M.; Andres, H.; Aebersold, M.; Borrás-Almenar, J. J.; Coronado, E.; Güdel, H. U.; Büttner, H.; Kearly, G. *Inorg. Chem.* **1997**, *36*, 2244.

(30) Andres, H.; Aebersold, M.; Güdel, H. U.; Clemente, J. M.; Coronado, E.; Büttner, H.; Kearly, G.; Zolliker, M. *Chem. Phys. Lett.* **1998**, *289*, 224.

(31) Andres, H.; Clemente-Juan, J. M.; Aebersold, M.; Güdel, H. U.; Coronado, E.; Büttner, H.; Kearly, G.; Melero, J.; Burriel, R. *J. Am. Chem. Soc.* **1999**, *121*, 10028.

(32) Andres, H.; Clemente-Juan, J. M.; Basler, R.; Aebersold, M.; Güdel, H. U.; Borrás-Almenar, J. J.; Gaita, A.; Coronado, E.; Büttner, H.; Janssen, S. *Inorg. Chem.*, **2001**, *40*, 1943.

(33) Palii, A. V.; Tsukerblat, B. S.; Coronado, E.; Clemente-Juan, J. M.; Borrás-Almenar, J. J. *Inorg. Chem.* **2003**, *42*, 2455.

(34) Palii, A. V.; Tsukerblat, B. S.; Coronado, E.; Clemente-Juan, J. M.; Borrás-Almenar, J. J. *J. Chem. Phys.* **2003**, *118*, 5566.

(35) Calvo-Perez, V.; Ostrovsky, S.; Vega, A.; Pelikan, J.; Spodine, E.; Haase, W. *Inorg. Chem.* **2006**, *45* (2), 644−649.

(36) Lines, M. E. *J. Chem. Phys.* **1971**, *55*, 2977.